

DEUTERIUM RETENTION IN THE MATERIAL OF WELDED SEAM RAFM STEEL EK-181 (RUSFER)

© 2025 A. V. Golubeva^{a,*}, A. P. Persianova^a, V. S. Efimov^b, N. P. Bobyr^a, and V. M. Chernov^{b, c}

^a*National Research Center “Kurchatov Institute”, Moscow, Russia*

^b*National Research Nuclear University “MEPhI”, Moscow Russia*

^c*JSC "Academician A.A. Bochvar High-Tech Research Institute of Inorganic Materials", Moscow, Russia*

*e-mail: av_golubeva@nrcki.ru

Received July 18, 2024

Revised December 25, 2024

Accepted January 30, 2025

Abstract. For the first time, deuterium retention in the welded seam of the domestic reduced-activation ferritic-martensitic (RAFM) steel EK-181 (Rusfer) was investigated in comparison with the usual samples of the same steel. The welded seam was obtained by the argon arc welding method of two sheets of steel EK-18 with a thickness of 2 mm. Samples were kept in gaseous deuterium at a pressure of 5 atmospheres and temperatures in the range of 623–773 K for 25 hours. The number of retained deuterium was determined by thermal desorption spectrometry (TDS). It was found that after exposure in the gas, samples carved from a weld retained about 2 times more deuterium than samples from conventional steel EK-181. The number of peaks in TDS spectra is the same for both ordinary steel and the area of the weld. The TDS spectra modeling was carried out using the TMAP7 code. The proposed model includes the presence of oxides on the surface and a high concentration of defects in the surface layer of samples, wherein well describing the experimental TDS spectra. The possible nature of hydrogen states in steel is discussed, which determines the features of TDS spectra.

Keywords: *RAFM steel, EK-181, Rusfer, welded seam, deuterium, retention, thermal desorption*

DOI: 10.31857/S00153230250213e8

1. INTRODUCTION

The DT fusion reaction is the simplest to implement in terrestrial conditions, so the first thermonuclear reactor (TNR) will operate on a mixture of deuterium and tritium. Radioactivity and the very high price of tritium are the reasons why hydrogen capture in TNR materials must be well predicted and reduced as much as possible. Therefore, the capture of hydrogen isotopes in TNR is the subject of intensive research by the thermonuclear community.

Low-activated ferritic-martensitic steels (LAFMS) are promising materials for nuclear reactors due to the relatively rapid decrease in activity induced by neutron irradiation. In the Russian Federation, EK-181 steel (Rusfer) has been developed and is being produced on an industrial scale

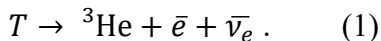
[1, 2] of this class. The advantages of this steel are good thermomechanical properties, as well as the widest range of operating temperatures among MAFMS: 573–973 K [6].

In metals, hydrogen can:

- be in a dissolved state, diffusing through the internodes;
- be captured in traps, which can be various structural defects – single vacancies, vacancy clusters, some impurities, dislocation loops, voids, etc.;
- form hydrides (in hydride-forming metals).

An important aspect of the use of structural materials in tokamak reactors is the inevitable presence of a large number of welded joints in contact with tritium. In particular, the total length of welded seams in one of the nine sectors of the ITER reactor vacuum chamber is 1.4 km [3]. The microstructure of welded seams obviously differs from the normal microstructure of the material being welded, therefore the concentrations of various defects in the seam will differ from those normal for the volume of the given material.

When solving the problem of ensuring mechanical stability of welded joints during reactor operation, one should also know how and to what extent the capture of hydrogen isotopes in the welded joint differs from retention in the regular material. This issue is important not only from the radiation safety perspective but also in terms of ensuring the required mechanical properties of the welded joint. The fact is that during the decay of radioactive tritium, radiogenic ${}^3\text{He}$ will be formed:



Helium has low mobility in the steel volume and forms helium bubbles, which leads to helium embrittlement. If tritium capture in the weld area is increased, degradation here will be accelerated.

A number of works [4-6] are devoted to the studies of hydrogen isotope capture in the domestic steel EK-181, however, hydrogen capture in the weld seam of EK-181 steel has not been previously studied. In fact, information about the capture of hydrogen isotopes in the welds of other RAFMs (Reduced Activation Ferritic/Martensitic Steels) is also absent, at least in the public domain.

The purpose of this work is to establish, through comparative research, how deuterium capture in the weld seam of EK-181 steel differs from capture in the bulk of this steel.

For the construction of thermonuclear reactors and research tokamaks, a number of welding methods are used, including electron beam welding [4], autogenous laser welding [5], arc welding, for example, tungsten arc welding [1]. Argon arc welding (also known as TIG welding from tungsten inert gas welding) is most commonly used in our country for welding vacuum elements because this method is relatively inexpensive, reliable, and does not require particularly high qualifications of the welder.

In this work, deuterium capture in the weld seam of EK-181 steel, obtained precisely by argon arc welding, was investigated.

2. MATERIAL AND SAMPLES

Steel EK-181 (Rusfer) is a RAFMS developed at the Bochvar Institute. V. Bochvar. The composition of EK-181 steel [6] in weight % is as follows: 0.16 C, 0.03 Ni, 0.07 N, 0.4 Si, 0.05 Ti, 0.4 V, 12 Cr, 0.6 Mn, 0.15 Ta, 1.09 W, with Fe as the main element.

Two plates were cut from a hot-rolled sheet of EK-181 steel with a thickness of 2 mm and butt-welded using argon arc welding. The width of the weld seam was 4 mm. The surface of the weld seam and adjacent areas was polished. It should be noted that during the cutting of samples, the stress-strain state of the material might have been partially altered.

The microstructure of the weld seam was investigated using an optical microscope, scanning electron microscope (SEM), and energy dispersive X-ray spectroscopy (EDS). Figure 1 shows the central area of the two butt-welded plates.

When describing a weld seam, researchers typically identify:

(I) the weld seam - an area that was completely melted during welding and is bounded by fusion lines;

(II) heat-affected zones (HAZ) adjacent to the weld seam. HAZ - areas where the microstructure has changed due to the steel being heated to temperatures above 673 K during welding. HAZ, in turn, can be divided into several areas depending on the temperature during welding and the resulting microstructure;

(III) the base material not subjected to thermal effects during welding.

Fig. 1. Surface of EK-181 steel samples, SEM data: (a) argon arc weld seam; (b) area inside the rectangle from Fig. 1a at higher magnification; (c) surface of EK-181 steel before welding, scanning electron microscope data.

Figure 1a shows the weld seam and part of the adjacent heat-affected zones. In the weld zone, there are individual large cavities with sizes up to fractions of millimeters. The boundary between the weld and the heat-affected zone at better resolution is shown in Fig. 1b. For comparison, the surface of the EK-181 steel rolled sample is shown in Fig. 1c. It can be seen that the microstructures of the surface in the weld area, heat-affected zone, and original material differ. In the welding zone, we see a coarse-grained structure. According to [7], a feature of 12 %-chromium steels, including EK-181 steel, is the formation of a high-strength martensite structure in the weld seam zone. The formation of high-strength martensite is characteristic of weldable RAFMS. The argon arc weld of the Chinese RAFMS CLAM also consisted of hardened martensite [8].

In the heat-affected zone, the grains are smaller than in the weld area, but larger and more pronounced than in the regular material (Fig. 1b). At the boundary between the weld area and the HAZ area, there is a high concentration of cavities with characteristic sizes \sim of 10 μm .

Samples were cut from the central part of the weld seam in such a way that the sample volume belonged to the weld zone. After mechanical polishing of all surfaces, the sample dimensions were $2 \times 2.5 \times 9.5$ mm. Samples of the same geometry were cut from an EK-181 steel sheet with a thickness of 2 mm. All samples were cleaned with alcohol and annealed in vacuum at 773 K for 2 hours, which is our standard procedural preparation of PASDPMS samples to reduce the concentration of defects formed in the near-surface layer during polishing [9].

Fig. 2. Different areas of the weld seam. SEM images.

According to microscopy data, at higher magnification (Fig. 2), cavities smaller than 0.5 μm are present in the weld volume, and their concentration varies in different areas of the weld.

Using EDS, it was determined that on the surface of the polished weld:

- the main elements in the weld zone are Fe (82 wt. %), Cr (10 wt. %), W (0.9 wt. %), as well as carbon (at least 5 wt. %) and Mn (0.8 wt. %);
- W, Fe and C, Ni, N, Si, Ti, V, Mn, Ta are distributed uniformly;
- the only element showing inclusions is chromium.

The content of Fe, Cr, W, Mn, determined by EDS, is close to expected. The high carbon content is probably related to the conditions under which the analysis was conducted: carbon tape is used to secure samples on the stage of the scanning electron microscope, therefore, carbon compounds must be present in the vacuum chamber of this equipment.

4. DESCRIPTION OF EXPERIMENTS

4.1. EXPOSURE IN GASEOUS DEUTERIUM

Exposure in gaseous deuterium was carried out on a high-vacuum stand with a special module for gas exposure with a volume of 130 cm^3 , shown in Fig. 3. Its chamber can be evacuated to high vacuum and filled with gas. The pressure is registered by a baratron-type sensor, the readings of which do not depend on the type of gas. The chamber is externally surrounded by a heater, covered with an outer screen to reduce heat loss. The temperature inside the module is measured by a chromel-alumel thermocouple, with a maximum achievable temperature of 1200 K. The feedback heating system allows maintaining the temperature of samples exposed to gas at a set level with a deviation of no more than 1 K. The gas inlet line is equipped with a nitrogen trap.

Fig. 3. Module for exposing samples to gas: 1 - exposure chamber surrounded by an external screen; 2 - current leads of the heater; 3 - pressure sensor; 4 - gas inlet line with a nitrogen trap.

Samples of EK-181 steel and the weld of the same steel were paired and exposed to gaseous deuterium at a pressure of 5 atmospheres at temperatures in the range of 623-773 K for 25 hours.

The samples were placed in pairs in the module, the volume was evacuated to a pressure of 10^{-5} Pa . Then, while continuing to pump, the module was heated to the required temperature. After that, the pumping was stopped and the module was filled with gaseous deuterium to a pressure of $5 \cdot 10^{-5} \text{ Pa}$. Deuterium used in the experiments, according to measurements by a quadrupole mass spectrometer, had a purity of not less than 99.99% D₂. The duration of exposure to gas was 25 hours. During the experiments, the pressure deviated from the set value by no more than 2%.

According to [10], the hydrogen diffusion coefficient in EK-181 steel at the minimum temperature of our experiments, 673 K, is $2.3 \cdot 10^{-9} \text{ m}^2/\text{s}$ and increases with temperature. According to classical diffusion theory, the deuterium diffusion coefficient is $\sqrt{2}$ times smaller than the hydrogen diffusion coefficient. If a diatomic gas is brought into contact with one side of a flat membrane, the characteristic time $\tau_{1/2}$ for the permeating flow to reach half of its maximum value is [11]:

$$\tau_{1/2} = \frac{L^2}{7.2 D}, \quad (2)$$

where L is the membrane thickness, D is the diffusion coefficient.

For a membrane made of EK-181 steel with a thickness of 1 mm (half the thickness of our samples) at the lowest temperature of our experiments, $\tau_{1/2}$ would be $\sim 10^3 \text{ s}$, which is much less

than the exposure duration of our samples in the gas. Therefore, in all cases, saturation of the samples with deuterium throughout the entire depth was achieved.

Upon completion of the experiment, the module volume was pumped out and heating was stopped. After cooling, the samples were removed from the setup and stored in atmosphere until studied by thermal desorption spectroscopy (TDS).

4.2. TDS

Measurements of capture by TDS were carried out on an ultra-high vacuum setup described in [12]. The residual pressure in the chamber of the setup is 2×10^{-7} Pa. The sample temperature was measured with a W-Re thermocouple attached directly to the sample. During TDS measurements, the samples were heated to a temperature of 1550 K at a rate of 2 K/s. The partial pressure of deuterium-containing molecules HD, D₂, HDO, D₂O, as well as several others was recorded by a Pfeiffer Prisma QMS 200M1 quadrupole mass spectrometer. The quadrupole mass spectrometer was calibrated according to the gas flow from a calibrated volume filled with deuterium to a known pressure. The calibration is described in detail in [15].

In the present experiments, deuterium left the samples predominantly in the form of D₂ molecules, less than 7% in the form of HD molecules, and the contribution of desorption in the form of HDO and D₂O molecules was less than 1%. Therefore, when processing the results, only the measured flows of D₂ and HD molecules were taken into account.

5. EXPERIMENT RESULTS

Thermodesorption measurements were carried out 3.5-4 months after saturating the samples with deuterium. During this time, approximately a quarter of the deuterium trapped in defects had left the EK-181 steel sample [13].

TDS spectra of the weld samples are shown in Fig. 4 with bold lines, TDS spectra of regular samples - with thin lines. TDS of samples that were saturated in deuterium simultaneously at the same temperature are given in the same color. Deuterium release from the samples occurred in the temperature range of 450-1400 K.

Most of the TDS spectra consist of three peaks, the temperatures of which are summarized in Table 1. Compared to regular samples, the first peak for weld samples is shifted by 30 K to higher temperatures. The positions of the second and third peaks are the same for both types of samples.

Table 1. Temperature of TDS spectra peaks. Peaks are numbered in the order of their appearance during heating from low to high temperatures

Peak	Temperature, K	
	Regular material	Weld
I	640 – 670	670 – 715
II	750 – 800	760 – 790
III	1010 – 1015	1015 – 1020

In the classical approximation, it is assumed that each peak is caused by a specific state of hydrogen in the material. The higher the binding energy of hydrogen in this state, the higher the temperature at which hydrogen is released during sample heating. In general, for steels, apart from dissolution, hydrogen capture is characteristic in traps such as grain boundaries and interphase boundaries, dislocations and dislocation loops, vacancies, vacancy clusters, carbides, solid solutions of alloying elements, oxide films, and cracks [14]. The most significant types of traps for EK-181 are grain boundaries and chromium carbides [15]. The binding energy of interphase boundaries with hydrogen is $\sim 0.45\text{-}0.55\text{ eV}$ [16], [17], while carbides have a higher binding energy - $0.76\text{-}1.0\text{ eV}$ [18].

Fig. 4. TDS spectra of EK-181 steel samples exposed to deuterium at a pressure of 5 atmospheres: thin lines - regular samples, bold lines - welded joint.

When comparing TDS spectra of regular samples (thin lines in Fig. 4), a slight decrease in the first peak is observed with increasing temperature at which the gas exposure was performed. This can be explained by the fact that at higher temperatures, deuterium captured in a low binding energy trap can more easily escape it. The amplitude of the second peak of the same samples depends little on the exposure temperature, while the amplitude of the last peak is lowest at the minimum sample temperature during gas exposure – 623 K.

For weld samples, no clear dependence of peak amplitudes in TDS on the temperature of deuterium introduction into the sample is observed. This is likely because the weld area is heterogeneous, and concentrations of defects of the same type differ in samples cut from different parts of the weld.

Fig. 5. Dependence of the amount of deuterium trapped in samples on the temperature at which the samples were held in gaseous deuterium at a pressure of 5 atmospheres for 25 hours.

The total amount of deuterium contained in the samples was determined by integrating the thermal desorption spectra of D_2 and HD molecules. The obtained value was divided by the sample surface area for ease of comparison with literature data, since studies on hydrogen isotope trapping usually present results in the format $[\text{D}/\text{m}^2]$. The dependence of the amount of deuterium trapped in the samples on the temperature at which they were saturated with deuterium is shown in Fig. 5. Weld samples trapped 1.5-2 times more deuterium than regular samples under the same conditions. It can be assumed that the increased deuterium trapping in weld samples is associated with the formation of cavities inside the samples: deuterium can accumulate in gaseous form inside the cavities, be chemisorbed on their surfaces, and also be bound to dislocation loops accompanying such microstructural inhomogeneities as cavities. Considering that melting of the material occurred in the weld zone, accompanied by grain coarsening, it cannot be excluded that the diffusion coefficients and deuterium solubility in the weld area differ from those for the base material of EK-181 steel.

Higher trapping in the weld will need to be taken into account in fusion facilities that will operate on a mixture of deuterium and tritium - heavy isotopes of hydrogen, since due to the decay of tritium according to reaction (1), helium embrittlement of welds will occur faster than in the base material.

6. NUMERICAL MODELING OF DEUTERIUM TRAPPING IN EK-181 STEEL

6.1. INITIAL DATA FOR MODELING

Modeling of thermal desorption spectra was carried out using the TMAP7 program [19], in which hydrogen transport is calculated in a one-dimensional approximation. The processes of hydrogen diffusion in metal and its trapping in TMAP7 are described by the following system of equations:

$$\frac{\partial C(x,t)}{\partial t} = D(T(t)) \frac{\partial^2 C(x,t)}{\partial x^2} - \sum_{i=1}^k \frac{\partial C_{tr}^i(x,t)}{\partial t} + G(x,t); \quad (3)$$

$$\frac{\partial C_{tr}^i(x,t)}{\partial t} = \frac{D(T(t))}{\lambda^2} C(x,t) \frac{N_i(x,t) - \sum_{i=1}^k C_{tr}^i(x,t)}{N} - \alpha_{dt}^i \cdot C_{tr}^i(x,t), \quad (4)$$

where $C(x,t)$ is the concentration of hydrogen dissolved in the sample; $C_{tr}^i(x,t)$ is the concentration of hydrogen trapped in the i -th trap; N_i is the concentration of the i -th trap; $G(x,t)$ is the internal hydrogen source (usually associated with hydrogen ion implantation); D is the hydrogen diffusion coefficient in the given material, α_{dt}^i is the release rate of a hydrogen atom from the i -th trap. For TMAP7, the maximum possible number of traps is three.

Let's discuss the parameters used in the modeling.

The permeability of EK-181 steel was experimentally investigated in [13], in particular, the diffusion and solubility coefficients for the hydrogen isotope protium were obtained. We used this diffusion coefficient as a starting point in our modeling, taking into account the isotope effect correction [20]. The solubility coefficient allows estimating the amount of hydrogen dissolved in steel according to Sieverts' law $C = S(T) \cdot p^{1/2}$, where C is the hydrogen concentration under the sample surface in contact with gaseous hydrogen; S is the solubility coefficient; T is the temperature during sample saturation with hydrogen; p is the hydrogen pressure above the surface. For the temperature range of 623-773 K and gas pressure of $5 \cdot 10^5$ Pa, the corresponding concentration will be in the range of $7 \cdot 10^{-23} - 2 \cdot 10^{-24}$ D/m³.

Data from [6] indicate that in the near-surface layer of EK-181 (at a depth of 1-2 μm), the deuterium content is an order of magnitude higher than throughout the sample thickness. This may be related to deuterium trapping in traps near the sample surface that formed during cutting and polishing.

The beginning of active deuterium desorption from ~ 500 K after exposure of samples in gas is not typical for RAFMS. For example, for CLF-1 steel with a chromium content of 8.5%, desorption after exposure of samples in gas began at ~ 420 K [21]. The first attempts to model TDS spectra of EK-181 also indicated that desorption should start from ~ 450 K (will be shown later). The surfaces of stainless steels in contact with oxygen are covered with a layer of self-healing chromium oxide, which prevents corrosion. Oxide films on the metal surface when in contact with hydrogen reduce its flow deep into the material. The observed desorption delay during TDS is most likely due to the Cr_2O_3 oxide film formed on the surface of EK-181 samples, which serves as a barrier for deuterium release from the sample. Therefore, modeling was carried out assuming that the samples have an oxide-steel-oxide structure. An approximate estimate of the diffusion coefficient for Cr_2O_3 was taken from the work [22], where the diffusion coefficient was calculated theoretically. The oxide thickness was assumed to be 10 nm, which is consistent with X-ray photoelectron spectroscopy data on the oxide layer thickness for the MANET ferritic-martensitic steel [23] (10.3% Cr), which is similar to EK-181.

For deuterium-saturated samples, only the TDS experiment stage was modeled, in which the main process occurring on the surface is the recombination of deuterium atoms. The boundary conditions on the sample surface are determined by the recombination coefficient. For EK-181, the recombination coefficient is unknown, so as an initial approximation, data on the recombination coefficient for MANET [24] were used. Subsequently, the recombination coefficient was an adjustable parameter, which was varied to achieve the optimal match with the experimental spectrum.

The goal of modeling was to obtain a set of model TDS spectra as close as possible to those obtained experimentally using the same set of parameters.

6.2. MODELING OF TDS SPECTRA OF EK-181 SAMPLES

Experimental and the most closely describing modeled TDS spectra of EK-181 steel (not weld) for different exposure temperatures of samples in gas are presented in Fig. 6.

Fig. 6. Experimental and simulated TDS spectra of EK-181 steel samples exposed to D₂-gas at 623, 673, and 723 K.

The parameters used in the modeling are as follows:

- recombination coefficient $K_r = 1 \cdot 10^{-29} \cdot \exp(0.35/kT) \text{ m}^4/\text{s}$;
- deuterium diffusion coefficient in EK-181 steel $D = 0.85 \cdot 10^{-7} \cdot \exp(-0.165/kT) \text{ m}^2/\text{s}$;
- deuterium diffusion coefficient in the oxide film $D_{ox} = 2 \cdot 10^{-8} \cdot \exp(-0.65/kT) \text{ m}^2/\text{s}$.

These results were obtained assuming that the steel samples contained dissolved deuterium with a concentration of $\sim 1 \cdot 10^{24} \text{ D/m}^3$, and that there are traps near the sample surface with a binding energy of 0.75 eV. Their concentration was $1.5 \cdot 10^{-2}$ atomic fraction, and their depth extended to 1 μm . The trap occupancy in the near-surface layer for modeling the spectra shown in Fig. 6 was adjusted so that the deuterium concentration in them was on the same order of magnitude as the data from nuclear reaction analysis of the near-surface layer of EK-181 obtained at a temperature of 600 K [6] (the maximum temperature for which the deuterium concentration profile in EK-181 is known when saturated from gas). The exposure pressure in the gas at the same temperatures does not have a strong influence on the amount of accumulated hydrogen in EK-181 steel. It was shown in [4] that at deuterium pressures of 10^1 Pa and 10^4 Pa above the surface, the deuterium concentrations in the near-surface layer differed only by a factor of two. Therefore, the difference in saturation pressure in this work (10^5 Pa) and in [6] (10^4 Pa) is not significant. TDS spectra with and without traps in the near-surface layer are presented in Fig. 7.

Fig. 7. Influence of near-surface traps on the shape of the model TDS spectrum.

From Fig. 7, it can be seen that adding near-surface traps to the model gives a result closer to the experimental data – the ascending branch of the peak becomes sharper.

Deuterium desorption from the sample surface in the experiment begins at $\sim 450 \text{ K}$. To delay the beginning of desorption in the simulation, it is necessary to either introduce an oxide layer on the sample surface or simulate TDS spectra with two types of traps: one uniformly distributed and one near-surface. The simulation results for these two approximations compared to the experimental TDS spectrum are shown in Fig. 8. The first option allowed obtaining model spectra closer to the experimental ones, therefore a three-layer sample model was used in the simulation of EK-181 TDS spectra at different temperatures: oxide–steel–oxide.

Fig. 8. Simulated TDS spectra of deuterium without an oxide layer on the sample. The red color shows the TDS spectrum with one trap of uniform concentration, green color shows the TDS spectrum with the same uniform trap, but with an added second near-surface trap. Gray color shows TDS spectra at different concentrations of the near-surface trap (from maximum concentration (green color) to zero concentration (red color)).

6.3. FEATURES OF THE HIGH-TEMPERATURE REGION OF THERMAL DESORPTION SPECTRA

The third peak observed for EK-181 at temperatures of \sim 1000 K during TDS could not be modeled. The attempt to add a third type of trap with high binding energy (1.5 eV) to the simulation does not give satisfactory agreement between the simulation results and experimental data (Fig. 9).

Fig. 9. TDS spectrum with "strong trap" (ST), without ST and their sum. The sum of TDS spectra shows that the narrow peak at \sim 1000 K cannot be described by simply adding ST to the simulation.

Apparently, the third peak is not described in the classical theory of hydrogen diffusion in metals and may be due to reasons that cannot be taken into account in the TMAP7 program used for modeling. Probable causes of the "anomalous" peak may be:

- the appearance of new strong traps during the TDS experiment under conditions of rapid heating, which were not present before the start of the experiment. Such traps, for example, could be carbides: in EK-181 steel, chromium carbides precipitate when heated to 870–970 K [24];
- destruction of the Cr_2O_3 oxide layer under the influence of high temperatures or deuterium [25], which leads to a sharp acceleration of the release of the remaining deuterium from the sample;
- phase transition $\alpha \rightarrow \gamma$, that is, the beginning of the rearrangement of the crystal lattice of EK-181 from BCC to FCC. The phase transition in EK-181 begins at 1143–1175 K [26].

7. CONCLUSIONS

A comparative study of deuterium capture in samples of EK-181 steel and the weld of this steel obtained by argon arc welding was carried out. Deuterium was introduced into the samples by exposure to gas for 25 hours at a pressure of 5 atmospheres in the temperature range of 623–773 K.

It is shown that the weld samples capture 1.5–2 times more deuterium than regular samples.

Modeling of thermodesorption spectra of EK-181 steel was performed in the TMAP7 program for gas saturation temperatures of 623, 673, and 723 K. The influence of some parameters on the shape of the model spectra is discussed. The anomalous nature of the thermodesorption peak at \sim 1000 K is noted.

Optimal agreement between calculated and experimental TDS spectra was achieved under the following assumptions:

- the flat sample is covered on both sides with a layer of chromium oxide Cr_2O_3 with a thickness of 10 nm;
- deuterium is dissolved in the bulk of the steel;

– deuterium traps are present in the near-surface layer with a thickness of 1 μm due to cutting and polishing. Their concentration is $1.5 \cdot 10^{-2}$ at., and the binding energy of deuterium with these traps is 0.75 eV.

FUNDING

This work was carried out as part of the state assignment of the National Research Center "Kurchatov Institute".

CONFLICT OF INTERESTS

The authors of this work declare that they have no conflict of interest.

REFERENCES

1. *Ioltukhovskiy A.G., Leonteva-Smirnova M.V., Solonin M.I., Chernov V.M., Golovanov V.N., Shamardin V.K., Bulanova T.M., Povstyanko A.V., Fedoseev A.E.* Heat resistant reduced activation 12% Cr steel of 16Cr12W2VTaB type-advanced structural material for fusion and fast breeder power reactors // *J. Nucl. Mater.* 2002. P. 532–535.
2. *Chernov V.M., Leonteva-Smirnova M.V., Potapenko M.M., Budykin N.I., Devyatko Yu.N., Ioltukhovskiy A.G., Mironova E.G., Shikov A.K., Sivak A.B., Yermolaev G.N., Kalashnikov A.N., Kuteev B.V., Blokhin A.I., Loginov N.I., Romanov V.A., Belyakov V.A., Kirillov I.R., Bulanova T.M., Golovanov V.N., Shamardin V.K., Strebkov Yu.S., Tyumentsev A.N., Kardashev B.K., Mishin O.V., Vasiliev B.A.* Structural materials for fusion power reactors—the RF R&D activities // *Nucl. Fusion*. 2007. V. 47. P. 839–848.
3. *Kim H.S., Moon H.K., Park C.K., Jung Y.J., Ha M.S., Park S.H., Joo Y.M., Joo J.K., Kang S.G., Seo J.Y., Han Y.H., Lim N.J., Yoon B.H., Choi S.Y., Hwang H.S., Hong K.H., Ahn H.J., Lee Y.J., Kim B.C., Lee H.G., Jung K.J., Sa J.W., Choi C.H., Chung W.H., Kim H.K., Kim Y.G., Kim G.H., Hong Y.S., Martinez J.M., Martin A., Jing J., Privalov M., Xiang B., Lobinger F., Pedrosa N., Rodilla E., Utin Y., Mestic A., Jung Y.S., Tok J.Y.W., Park K.H., Kim H.C., Seok S.H., Park D.B., Moon G.H., Lee J.H., Lim K.S., Kim J.B., Yeo H.K., Lee J.J.* Manufacturing completion of the first ITER vacuum vessel sector // *Nucl. Fusion*. 2022. V. 63. 076044 (14 p).
4. *Shi Yi., Zhang G., Liao H., Wang Xi., Wu Sh.* Optimization of electron beam butt welding of 32 mm CLF-1 steel T-joints of Test Blanket Module (TBM) in ITER // *Fusion Eng. & Design* , 2020, V. 161 . P. 111931.
5. *Wen-Hua D., Yun-Tao S., Ji-Jun X., Chao F., Wei J., Wu J.F.* Investigation on the microstructure and mechanical properties of autogenous laser welding joint of ITER BTCC case lid // *Fus. Eng. &Design*. 2020. V. 156. P. 11160.
6. *Leonteva-Smirnova M.V., Agafonov A.N., Ermolaev G.N., Ioltukhovsky A.G., Mozhanov E.M., Reviznikov L.I., Tsvelev V.V., Chernov V.M., Bulanova T.M., Golovanov V.N., Ostrovsky Z.O., Shamardin V.K., Blokhin A.I., Ivanov M.B., Kozlov E.V., Kolobov Yu.R., Kardashev B.K.* Microstructure and mechanical properties of low-activation ferritic-martensitic steel EK-181 (RUSFER-EK-181) // *Perspective materials*. 2006. Vol. 6. P. 40–52.
7. *Leontieva-Smirnova M.V., Agafonov A.N., Mozhanov E.M., Chernov V.M.* Weldability of heat-resistant chromium (12%) steels EK-181 and ChS-139 // *Problems of atomic science and technology*, Ser. Fusion. 2011. Iss. 4. P. 14–21.
8. *Jiang Zh., Ren L., Huang J., Ju Xi., Wu H., Huang Q., Wu Y.* Microstructure and mechanical properties of the TIG welded joints of fusion CLAM steel // *Fusion Engineering and Design*, 2010. V. 85. P. 1903–1908.

9. *Golubeva A.V., Bobyr N.P., Cherkez D.I., Gasparyan Yu.M., Khripunov B.I., Klimov N.S., Spitsyn A.V., Chernov V.M.* Hydrogen isotopes interaction with ferritic-martensitic steel Ek-181(Ek-181-Rusfer): Review of results obtained // Perspective materials. 2021. No 4. P. 5–18.
10. *Danilov I.V., Kapyshev V.K., Kovalenko V.G., Kalashnikov A.N.* Facility for studies of structural materials permeability to hydrogen isotopes // Questions of atomic science and technique, Ser. Fusion. V. 37. Iss. 2. P. 38–44.
11. *Bekman I.N.* Mathematical apparatus of diffusion, Moscow, Yurait, 2019. 95 p.
12. *Rusinov A.A., Gasparyan Y.M., Pereygin S.F., Pisarev A.A., Stepanov S.O., & Trifonov N.N.* A setup for thermodesorption measurements. Instruments and Experimental Techniques, 2009. V. 52. P. 871–876.
13. *Golubeva A.V., Alimov V.Kh., Efimov V.S., Bobyr N.P., Kozlov D.A.* Influence of storage conditions on deuterium release from low-activation ferritic-martensitic steels // Surface, X-ray, synchrotron and neutron research. 2024. (in press)
14. *Koyama M., Rohwerder M., Tasan C.C., Bashir A., Akiyama E., Takai K., Raabe D., Tsuzaki K.* Recent progress in microstructural hydrogen mapping in steels: quantification, kinetic analysis, and multi-scale characterisation // Materials Science and Technology. 2017. V. 33. № 13. P. 1481–1496.
15. *Alimov V.Kh.* Irradiation of reduced-activation ferritic-martensitic steels with deuterium plasma. Review of data on surface modification, diffusion, and deuterium accumulation // Journal of Surface Investigation: X-ray, Synchrotron and Neutron Techniques. 2024. (in press)
16. *Wu W., Zhang X., Li W., Fu H., Liu S., Wang Y., Li J.* Effect of hydrogen trapping on hydrogen permeation in a 2205 duplex stainless steel: Role of austenite–ferrite interface // Corrosion Science. 2022. V. 202. P. 110332.
17. *Frappart S., Feaugas X., Creus J., Thebault F., Delattre L., Marchebois H.* Study of the hydrogen diffusion and segregation into Fe–C–Mo martensitic HSLA steel using electrochemical permeation test // Journal of Physics and Chemistry of Solids. 2010. V. 71. № 10. P. 1467–1479.
18. *Mizuno M., Anzai H., Aoyama T., Suzuki T.* Determination of hydrogen concentration in austenitic stainless steels by thermal desorption spectroscopy // Materials Transactions, JIM. 1994. V. 35. № 10. P. 703–707.
19. *Longhurst G.R.* TMAP7 User Manual // Idaho National Laboratory (INL). 2008. 79 p.
20. *Shishkova T., Golubeva A., Rozenkevich M.* Isotope effect in the interaction of hydrogen with materials of thermonuclear reactors // Russian Journal of Physical Chemistry A. 2023. V. 97. № 10. P. 1371–1392.
21. *Xu Yu-P., Lu T., Li Xi.-Ch., Liu F., Liu H.-D., Wang J., An Zh.-Q., Ding F., Hong S.-H., Zhou H.-Sh., Luo G.-N.* Influence of He ions irradiation on the deuterium permeation and retention behavior in the CLF-1 steel // Nuclear Instruments and Methods in Physics Research Section B: Beam Interactions with Materials and Atoms. 2016. V. 388. P. 5–8.
22. *Chen C.F., Yu H.B., Zheng S.Q.* First-principles study of hydrogen diffusion mechanism in Cr₂O₃ // Science China Technological Sciences. 2011. V. 54. P. 88–94.
23. *Serra E., Perujo A.* Influence of the surface conditions on permeation in the deuterium–MANET system // Journal of nuclear materials. 1997. V. 240. № 3. P. 215–220.
24. *Arbuzov V.L., Voronin V.I., Goshchitsky B.N., Danilov S.E., Kazantsev V.A., Kataeva N.V., Sagaredze V.V.* Features of structural-phase states and physical properties of ferritic-martensitic steel EK-181 after various heat treatments // Problems of Atomic Science and Technology. Series: Materials Science and New Materials. 2015. № 1. P. 8–21.
25. *Katsuta H., Furukawa K.* Hydrogen and deuterium transport through type 304 stainless steel at elevated temperatures // Journal of Nuclear Science and Technology. 1981. V. 18. № 2. P. 143–151.
26. *Chernov V.M., Leontieva-Smirnova M.V., Potapenko M.M., Polekhina N.A., Litovchenko I.Yu., Tyumentsev A.N., Astafurova E.G., Khromova L.P.* Structural-phase transformations and physical properties of ferritic-martensitic 12% chromium steels EK-181 and ChS-139 // Journal of Technical Physics. 2016. V. 86. № 1. P. 99–104.